Individual-level fMRI Segmentation Based on Graphs

Kevin W. Tong, Xiao-Yan Zhao, Yong-Xia Li, Ping Li, *Member, IEEE*

***Abstract*—Aiming at the high complexity of fMRI data and the great spatial dependence of existing methods, a whole-brain functional segmentation algorithm with low computational overhead and low spatial structure dependence is proposed for individual-level fMRI segmentation in 3D space. Firstly, the spatial information and functional connectivity of each voxel in fMRI are utilized for pre-segmentation to create compact and functionally consistent super voxels, then extracts features such as average spatial coordinates and average time series at the super voxel level to reduce the computational effort of the segmentation algorithm, and performs segmentation in a cut-free manner to obtain the optimal segmentation graph by minimizing the energy function. The results of contrast experiment demonstrated that the algorithm fully exploits the connectivity information of fMRI for segmentation, relies less on the spatial structure, and achieves better functional segmentation results, which is an effective whole-brain functional segmentation method.**

I. Introduction

NEUROS can be used as nodes in the brain functional network to explore the connection relationships among neurons. Each neural component controlling different neural activities can also be regarded as brain network nodes to study the correlation between the nervous. For the four-dimensional fMRI data, each voxel value represents the blood oxygenation level dependent (BOLD) signal intensity of the corresponding region of the brain at the current time point, so it is possible to set voxels as nodes of the network and the connectivity between voxels as the edges of the network, thus developing a high-dimensional brain functional network. Nevertheless, for many types of connectivity analysis, high-resolution fMRI has a huge amount of data, which is often computationally infeasible and may contain much noise, making subsequent network analysis difficult to carry out [1]–[3]. At present, a better solution is to subdivide the brain into a certain number of non-overlapping brain regions in the spatial domain, where each brain region contains a certain number of voxels and is defined as a node connecting to the network. In this way, the number of nodes in the brain network is equal to the number of brain regions.

To construct functional brain networks regarding brain regions as nodes, resting-state fMRI is usually segmented into a certain number of brain regions by predefined mapping or segmentation algorithms. Next, the correlations between the brain regions are calculated and merged into an adjacency matrix. This adjacency matrix represents the functional network of the brain, which elucidates the pathways through which regions are structurally connected or functionally coupled in the resting state of the brain. This method of building a functional brain network both allows for control of the brain network complexity and facilitates the study of the functional connectivity between different regions of the brain. By defining a functional brain network, the corresponding BOLD signals in every brain region can be analyzed, and the association between the activation of brain regions and age, gender, cognition, and various brain diseases can be researched [4]–[7]. In summary, it is clear that proposing an effective brain modeling method and then accurately segmenting each brain region is of great significance for further understanding human physiological cognitive processes as well as for analyzing and diagnosing brain-related diseases. Hence, this paper implements research on modeling and analysis of brain functional network for resting-state fMRI, aiming to explore a rational and more efficient segmentation methods of brain function.

Brain networks based on functional brain segmentation are widely used for fMRI analysis and disease diagnosis tasks [8]–[10]. Fan et al [11] designs a connection-based segmentation framework, which recognizes the subdivision of the whole human brain and reveals the connection structure. However, the existing segmentation algorithms have the following problems: (1) Most studies related to brain segmentation only segment one or a few ROIs such as hippocampus and cingulate cortex, and it may be difficult to extend the segmentation to the whole brain. (2) Some functional brain segmentation algorithms target the entire cerebral cortex, but the segmentation is often done on the brain surface, ignoring subcortical regions and the potential correlations between left and right brain regions. (3) Brain segmentation usually relies on the structural information of the brain and ignores the connectivity information of the brain, which does not realize the real functional brain segmentation. Although graph-based methods can preserve the structural information of brain maps, the training efficiency is often low because the connections in the brain map are complicated. In addition, many methods are not interpretable and cannot explain the reasons for the superiority and inferiority of brain graph classification effects.

The main contributions of this work are as follows: (1) An individual-level fMRI segmentation algorithm ISFC-GWC with low parametric number and low spatial dependence is

(Corresponding authors: Ping Li.)

Kevin W. Tong is with the Nanjing University of Science and Technology, Jiangsu 210094, China. (e-mail: tongwei@njust.edu.cn).

Xiao-Yan Zhao is with Rehabilitation Medicine, Anhui No.2 Provincial People's Hospital, Hefei 230041, China (e-mail: zxy364@163.com).

Yong-Xia Li is with the Department of Emergency, Shanghai sixth people's hospital, Shanghai 200000, China. (e-mail: liyongxia2021@163.com).

Ping Li is with the School of Biological Science and Medical Engineering, Beihang University, Beijing 100191, China. (e-mail: liping@buaa.edu.cn).

raised to achieve whole-brain functional segmentation in 3D-volume space. (2) The algorithm introduces cut-free maps into the segmentation of four-dimensional fMRI data and minimizes the objective function by iterative optimization. (3) Experiments and comparative analysis with other connection-driven segmentation algorithms were conducted using fMRI of a healthy population, which validates that the ISFC-GWC algorithm is an effective solution for individual-level functional brain segmentation.

II. Methods

A. ISFC-GWC Brain Function Segmentation Algorithm

For fMRI segmentation, the spatial and functional features of fMRI are first extracted at the super voxel level, then the energy minimization function is constructed through GWC, and neighborhood nodes are adaptively assigned to each super voxel based on the feature matrix to learn the correlation map between super voxels. Specifically, after the super voxels are obtained by the ISFC algorithm, manual feature extraction is performed at the super voxel level, and the corresponding feature matrix is created, then the feature matrix is input to the cut-free graph algorithm to construct and segment correlation graph at the super voxel level. Assuming that all voxels in the gray matter part are clustered into N super voxels by the aforementioned super voxel generation algorithm, and H features are extracted manually for each super voxel. As a result, a matrix can be constructed for each feature as follows.

$$F^{(h)} = [\mathbf{f}_1^{(h)}, \mathbf{f}_2^{(h)}, ..., \mathbf{f}_{\mathrm{N}}^{(h)},] \in \mathbb{R}^{d_h \times \mathrm{N}}, \quad h = 1, 2, ..., \mathrm{H}, \quad (1)$$

where d_h denotes the dimensionality of the feature. P denotes the average of 3D coordinates in the image space of all voxels in each super voxel, then there is

$$P = [\mathbf{p}_1, \mathbf{p}_2, ..., \mathbf{p}_{\mathrm{N}}] \in \mathbb{R}^{3 \times \mathrm{N}}. \quad (2)$$

The idea of the cut-free graph algorithm is to learn a correlation graph based on the extracted feature matrix $G \in \mathbb{R}^{\mathrm{N} \times \mathrm{N}}$, which reflects the correlation between the super voxels. This graph has K connected components and is obtained by developing an energy minimization problem [12]. Since the connection-driven segmentation-based approach uses both spatial as well as functional information of the fMRI data, and an optimal correlation map should be smooth over different spatial and functional feature information. Hence, it is essential to define two cost functions $s(G, P)$ and $c(G, F)$ which are used to measure the smoothness of graph G over spatial and feature information respectively. Additionally, a separate penalty term needs to be defined to balance the significance between different features. Therefore, the optimization function for solving the optimal graph G can be defined as

$$\min_{G, \boldsymbol{\delta}} s(G, P) + \alpha \sum_{h=1}^{\mathrm{H}} \delta^{(h)} c(G, F^{(h)}) + \lambda r(G, \boldsymbol{\delta}), \quad (3)$$

where α and λ are parameters that respectively regulate the balance between different items, and $\delta^{(h)}$ represents the parameters that balance the distinct features. $\boldsymbol{\delta} = [\delta^{(1)}, \delta^{(2)}, ..., \delta^{(\mathrm{H})}] \in \mathbb{R}^{\mathrm{H}}$ and $r(G, \boldsymbol{\delta})$ are the penalty terms defined on the graphs G and $\boldsymbol{\delta}$. For these penalty terms, this paper refers to [13] and defines them as

$$r(G, \boldsymbol{\delta}) = \| G \|_F^2 + \beta \| \boldsymbol{\delta} \|_2^2, \quad (4)$$

where $\| \cdot \|_F$ denotes the F-norm of the matrix. The constraint $\delta \geq 0$ and $\boldsymbol{\delta}^T \mathbf{1} = 1$ is set on $\boldsymbol{\delta}$, i.e., let the weight coefficients of all features be between $[0, 1]$ and sum to 1.

Based on the two cost functions defined between graph G and the spatial information P and the feature information F, it is considered that the super voxels with higher similarity are more likely to be in the same functional partition and their corresponding edges in graph G should have higher weights. The graph is represented in the form of a matrix, and each element in G can be viewed as the weight or probability of the edge connecting the nodes of the corresponding two super voxels, so the cost function can be defined as

$$s(G, P) = \sum_{i,j=1}^{\mathrm{N}} \| \mathbf{p}_i - \mathbf{p}_j \|_2^2 \, g_{ij}, \quad (5)$$

$$c(G, F^{(h)}) = \sum_{i,j=1}^{\mathrm{N}} \| \mathbf{f}_i^{(h)} - \mathbf{f}_j^{(h)} \|_2^2 \, g_{ij}. \quad (6)$$

All the Euclidean distances are used to express the level of similarity between the super voxels' spatial information and the feature information. g_{ij} denotes the edge weights connecting super voxels i and j in graph G. Furthermore, a constraint is added to the edges in graph G.

$$\mathbf{g}_j^T \mathbf{1} = 1, \ g_{ij} \geq 0, \ i, j = 1, 2, ..., \mathrm{N}. \quad (7)$$

Combining the above equations, the objective function can be obtained via replacing the penalty term and the cost function in Equation (3) by Equations (4), (5), and (6), respectively.

$$\begin{aligned} \min_{G, \boldsymbol{\delta}} & \sum_{i,j=1}^{\mathrm{N}} \| \mathbf{p}_i - \mathbf{p}_j \|_2^2 \, g_{ij} \\ & + \alpha \sum_{h=1}^{\mathrm{H}} \sum_{i,j=1}^{\mathrm{N}} \delta^{(h)} \| \mathbf{f}_i^{(h)} - \mathbf{f}_j^{(h)} \|_2^2 \, g_{ij} \\ & + \lambda \| G \|_F^2 + \lambda \beta \| \boldsymbol{\delta} \|_2^2, \\ s.t. & \begin{cases} \mathbf{g}_j^T \mathbf{1} = 1, \ g_{ij} \geq 0, \ i, j = 1, 2, ..., \mathrm{N}; \\ \boldsymbol{\delta}^T \mathbf{1} = 1, \ \delta \geq 0. \end{cases} \end{aligned} \quad (8)$$

If there is no penalty term $r(G, \boldsymbol{\delta})$, In the original problem, each super voxel can obtain the optimal solution by selecting only the super voxel with the highest similarity as the neighbor and setting the corresponding edge probability to 1, but this is not rational. Instead, the optimal solution for $\min \| G \|_F^2$ in this penalty term is that all super voxels are connected to the current super voxel with the same probability. Hence, this term can be equivalent to a priori information about the connection [14], and the same for the term $\| \boldsymbol{\delta}_2^2 \|$.

This optimization task is expected to segment the fMRI into K functional brain regions, so ideally there are K connected components in graph G obtained from optimization. However, the optimal solution obtained by the usual equation 8 cannot satisfy the ideal situation. Therefore, in order to make the number of connected components of graph G adaptive to

the preset number of partitions K, it is necessary to add a constraint on the edges' weights g_{ij} in the graph. Assuming that each node i in the graph is assigned a function-valued vector $\mathbf{y}_i \in \mathbb{R}^{\mathrm{K}}$, then all nodes form a function-valued matrix $Y = [\mathbf{y}_1, \mathbf{y}_2, ..., \mathbf{y}_N]^T \in \mathbb{R}^{\mathrm{N}\times\mathrm{K}}$ and $Y^TY = I$, there is

$$\begin{aligned}\sum_{i,j=1}^{\mathrm{N}} \parallel \mathbf{y}_i - \mathbf{y}_j \parallel_2^2 g_{ij} &= 2tr\left(Y^T\left(D_G - \frac{G+G^T}{2}\right)Y\right) \\ &= 2tr\left(Y^T L_G Y\right),\end{aligned} \tag{9}$$

where $tr(\cdot)$ denotes the trace of the matrix. $D_G \in \mathbb{R}^{\mathrm{N}\times\mathrm{N}}$ is the degree matrix, which is defined as a diagonal matrix whose first i diagonal element is $\sum_{j=1}^{\mathrm{N}}(g_{ij}+g_{ji})/2$. $L_G = D_G - \frac{G+G^T}{2}$ refers to the Laplacian matrix of the graph G. The graph G is a nonnegative matrix, so the number K of connected components in G is equal to the number of zero eigenvalues in L_G [15]. And since the Laplacian matrix can be similarly diagonalized, if the rank of L_G is equal to $\mathrm{N}-\mathrm{K}$, it would have $\mathrm{N}-\mathrm{K}$ non-zero eigenvalues, then the graph G has K connected components. As a result, in order to obtain segmentation results with a predetermined functional partition, it is necessary to add a rank constraint to G in equation 8, so the updated optimization problem is

$$\begin{aligned} f_{opt} = \min_{G,\boldsymbol{\delta}} & \sum_{i,j=1}^{\mathrm{N}} \parallel \mathbf{p}_i - \mathbf{p}_j \parallel_2^2 g_{ij} \\ & + \alpha \sum_{h=1}^{\mathrm{H}} \sum_{i,j=1}^{\mathrm{N}} \delta^{(h)} \parallel \mathbf{f}_i^{(h)} - \mathbf{f}_j^{(h)} \parallel_2^2 g_{ij} \\ & + \lambda \parallel G \parallel_F^2 + \lambda\beta \parallel \boldsymbol{\delta} \parallel_2^2, \\ s.t. \ & \begin{cases} \mathbf{g}_j^T\mathbf{1} = 1, \ g_{ij} \geq 0, \ i,j = 1,2,...,\mathrm{N}; \\ \boldsymbol{\delta}^T\mathbf{1} = 1, \ \delta \geq 0; \\ rank(L_G) = \mathrm{N}-\mathrm{K}, \ L_G = \frac{G+G^T}{2}. \end{cases} \end{aligned} \tag{10}$$

Because L_G in the constraint of Equation 10 relies on G which needs to be solved, the problem is difficult to optimize. However,L_G is a semi-positive definite matrix and its eigenvalues are all non-negative, so the penalty term can be added to the objective function to make L_G the smallest K eigenvalues $\sigma(L_G)$ approaching 0. Based the proof in [14], there is

$$\sum_{i=1}^{K} \sigma_i(L_G) = \min_{Y^TY=I} tr(Y^T L_G Y), \tag{11}$$

therefore, equation (10) is equivalent to

$$\begin{aligned} f_{opt} = \min_{G,\boldsymbol{\delta}} & \sum_{i,j=1}^{\mathrm{N}} \parallel \mathbf{p}_i - \mathbf{p}_j \parallel_2^2 g_{ij} \\ & + \alpha \sum_{h=1}^{\mathrm{H}} \sum_{i,j=1}^{\mathrm{N}} \delta^{(h)} \parallel \mathbf{f}_i^{(h)} - \mathbf{f}_j^{(h)} \parallel_2^2 g_{ij} \\ & + \lambda \parallel G \parallel_F^2 + \lambda\beta \parallel \boldsymbol{\delta} \parallel_2^2 + 2\eta \sum_{i=1}^{\mathrm{K}} \sigma_i(L_G), \\ s.t. \ & \begin{cases} \mathbf{g}_j^T\mathbf{1} = 1, \ g_{ij} \geq 0, \ i,j = 1,2,...,\mathrm{N}; \\ \boldsymbol{\delta}^T\mathbf{1} = 1, \ \delta \geq 0. \end{cases} \end{aligned} \tag{12}$$

According to equation (9), equation (12) is further equivalent to

$$\begin{aligned} f_{opt} = \min_{G,\boldsymbol{\delta},Y} & \sum_{i,j=1}^{\mathrm{N}} \parallel \mathbf{p}_i - \mathbf{p}_j \parallel_2^2 g_{ij} \\ & + \alpha \sum_{h=1}^{\mathrm{H}} \sum_{i,j=1}^{\mathrm{N}} \delta^{(h)} \parallel \mathbf{f}_i^{(h)} - \mathbf{f}_j^{(h)} \parallel_2^2 g_{ij} \\ & + \eta \sum_{i,j=1}^{\mathrm{N}} \parallel \mathbf{y}_i - \mathbf{y}_j \parallel_2^2 g_{ij} \\ & + \lambda \parallel G \parallel_F^2 + \lambda\beta \parallel \boldsymbol{\delta} \parallel_2^2, \\ s.t. \ & \begin{cases} \mathbf{g}_j^T\mathbf{1} = 1, \ g_{ij} \geq 0, \ i,j = 1,2,...,\mathrm{N}; \\ \boldsymbol{\delta}^T\mathbf{1} = 1, \ \delta \geq 0; \\ Y^TY = I_{\mathrm{K}}, \ Y \in \mathbb{R}^{\mathrm{N}\times\mathrm{K}}. \end{cases} \end{aligned} \tag{13}$$

The value of η should be taken as large as possible to force the term to 0.

B. ISFC Super Voxel Generation Algorithm

To make the functional segmentation at the super voxel level meaningful, in the super voxel generation process, the correlation measure of the BOLD signal between voxels is introduced and the spatial distance is combined for iteration, so as to guarantee that all voxels in the generated super voxels are connected and have similar functional signals. Moreover, during the iterative update of the ISFC algorithm, only the M voxels with the closest joint spatial functional distance to each voxel are fuzzily associated. Specifically, assuming that the predefined number of super voxels to be generated is K, then K seed points are first initialized, i.e., clustering centers. In order to makes the seed points evenly distributed in the image and gets the super voxels with the same size, assuming that there are totally N voxels, then the size of each super voxel should be N/K, so the distance between adjacent cluster centers should be $\sqrt[3]{\mathrm{N}/\mathrm{K}}$. Based on this step, the initialized clustering centers are obtained by initializing the seed points in the three-dimensional space and keeping the seed points belonging to the gray matter region. The clustering centers obtained by this initialization method are uniformly distributed in space.

After confirming the initialized K clustering centers, each cluster center $c_i, i \in \{1,2,...,\mathrm{K}\}$ is represented by a vector consisting of spatial coordinate and a time series of BOLD signals stitched together

$$c_i = [x_i, y_i, z_i, \mathbf{b}_i^T]^T \in \mathbb{R}^{3+T}, \tag{14}$$

where T is the number of time points in the fMRI data, and x_i, y_i, z_i are the coordinates of the clustering center c_i in the three-dimensional space, $\mathbf{b}_i$ is the average time series of BOLD signals in the $3\times3\times3$ neighborhood of c_i. The average intensity of neighboring voxels is utilized to initialize the clustering centers to weaken the impact of noise.

Next, for each voxel in the gray matter region, it is only fuzzily associated with M spatially closest cluster centers $S =$

$\{s_1, s_2, ..., s_{\mathrm{M}}\}$, and the corresponding fuzzy affiliation degree is calculated as follows.

$$a_{ij} = \frac{(1/d(v_i, c_j))^{\frac{2}{\alpha-1}}}{\sum_{m=1}^{\mathrm{M}}(1/d(v_i, c_m))^{\frac{2}{\alpha-1}}}, \ j \in S, \tag{15}$$

where a_{ij} denotes the fuzzy affiliation between voxel i and clustering center j, $v_i \in \mathbb{R}^{3+\mathrm{T}}$ is likewise the spatial and intensity information of voxel i represented by a vector. α is a fuzzification parameter to control the sensitivity of noise [16], and $d(v_i, c_j)$ is a measure of the predefined distance between v_i and c_j. This leads to $a_{ij} \in (0, 1)$ and the sum of the affiliation of voxel v_i to the M nearest clustering centers is 1. Local clustering in this way can overcome the problem of non-uniformity of fMRI intensity, and reduce the computational effort required for fuzzy affiliation calculation when obtaining super voxels with better shapes. During the process of finding the M nearest clustering centers, it is not efficient sufficiently to find them by calculating the distance to all clustering centers for each voxel. To reduce the computational effort, the P nearest prime centers to each clustering center are first calculated and the nearest clustering center is marked for each voxel during each iteration. Then for each voxel, M clustering centers are selected from the nearest clustering center as well as its neighborhood P centers. For the distance metric between voxels and clustering centers, spatial distance and functional similarity are combined to define.

$$\begin{aligned} d(v_i, c_j) &= \lambda d_{space}(v_i, c_j) + d_{similarity}(v_i, c_j) \\ &= \lambda\sqrt{(x_i - x_j)^2 + (y_i - y_j)^2 + (z_i - z_j)^2} \\ &\quad + \parallel \mathbf{b}_i - \mathbf{b}_j \parallel_2, \end{aligned} \tag{16}$$

In the equation above, λ is used to normalize the spatial distance to the same scale as the functional distance, and the normalized Euclidean distance is equivalent to the Pearson correlation coefficient, so both the spatial and functional distances are defined using the Euclidean distance. Therefore, the objective function requiring to be minimized by the final super voxel generation algorithm is

$$f = \sum_{i=1}^{\mathrm{N}}\sum_{j=1}^{\mathrm{M}} a_{ij}^{\alpha} d(v_i, c_j), \tag{17}$$

After fuzzily associating all voxels to their M nearest cluster centers, new cluster centers are calculated.

$$c_j^{(t+1)} = \frac{\sum_{l=1}^{N_j} a_{lj}^{\alpha} \cdot c_j^{(t)}}{\sum_{l=1}^{N_j} a_{lj}^{\alpha}} \in \mathbb{R}^{3+\mathrm{T}}, \tag{18}$$

where N_j is the number of voxels fuzzily associated with cluster center j. $c_j^{(t)}$ and $c_j^{(t+1)}$ respectively denote the current and updated cluster center vector representations.

As a result, the objective function is optimized iteratively during the voxel update as well as the fuzzy clustering center update, and the residual refers to the distance between the clustering centers before and after the update. Algorithm 1 describe the algorithm implementation in detail. Note that in this paper, experiments are carried out on a small fMRI dataset [17] published by Southeast University, which includes fMRI data collected by 40 healthy college students at rest.

Algorithm 1 Super voxel generation algorithm flow based on ISFC

1: Input: fMRI data, preset number K of super voxels and residual threshold ε
2: Output: super voxel generation results
3: initialize K clustering centers and denote the center of mass by vector $c_i = [x_i, y_i, z_i, \mathbf{b}_i^T]^T \in \mathbb{R}^{3+\mathrm{T}}$, $i = 1, 2, ..., \mathrm{K}$ respectively
4: define the distance and objective functions by equations (16) and (17)
5: **repeat**
6: **For** each voxel in the gray matter region
7: calculate its affiliation degree with the M closest clustering centers in space at the current moment by equation (15)
8: **end for**
9: update the K clustering centers by equation (18)
10: **until** $max_j \left\{ \parallel c_j^{(t+1)} - c_j^{(t)} \parallel_2 \right\} < \varepsilon$
11: calculate the latest fuzzy affiliation degree and assign each voxel to the clustering center with the largest affiliation

III. Results

A. Super Voxel Generation based on Iterative Clustering of Spatial Functionality

Super voxel refers to sub-region with consistent local features generated by clustering similar voxels in a 3D image. This region aggregates voxels with feature redundancy into meaningful super voxels, thus reducing the dimensionality of the original image [18]. Specifically for fMRI segmentation tasks, super voxel generation is the segmentation of fMRI into several small regions with uniform and compact appearance, then execute fMRI processing and analysis at the super voxel level. This paper introduces a new spatial fuzzy clustering algorithm [19] for super voxel generation of fMRI data, and extends it to the pre-segmentation task of four-dimensional fMRI data, consequently proposing the Iterative Spatial Functional Clustering (ISFC) super voxel generation algorithm in this paper for fMRI super voxel generation.

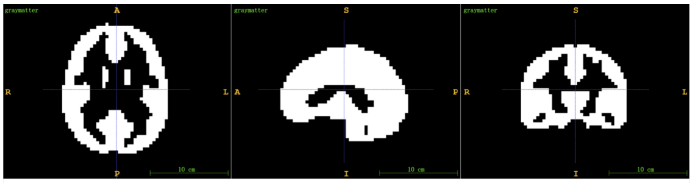

Fig. 1: Gray matter template

Since fMRI data often have high dimensionality, it is very computationally intensive to segment them directly at the voxel level. Therefore, the ISFC super voxel generation algorithm was utilized in this paper to first generate the corresponding super voxels for the 40 subjects' fMRI on the gray matter template as shown in Figure 1, which reduced the dimension of the original fMRI data. The gray matter template contained a total of 18384 voxels, and the number of super voxels K

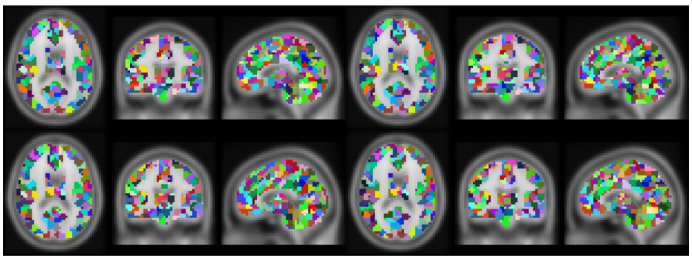

Fig. 2: Brain maps by super voxel generation

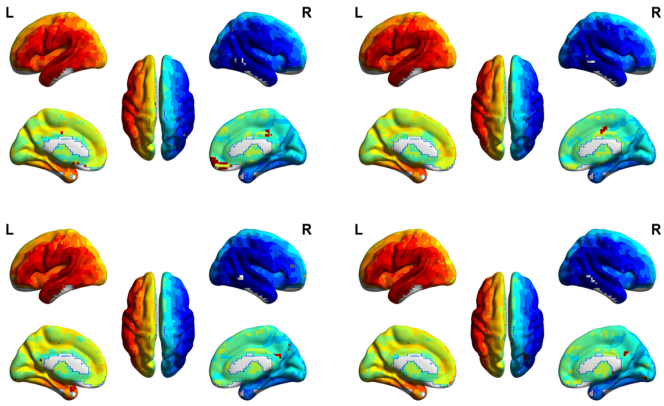

Fig. 3: Super voxels mapped onto the brain surface

was preset to 1000, so that each super voxel obtained included about twenty voxels on average. According to the super voxel generation algorithm, the residual threshold ε was set to 0.001 and the number of nearest cluster centers M was set to 4.

Figures 2 and 3 show the super voxel generation results of four subjects when the predetermined number of super voxels is 1000, and the corresponding segmentation results are mapped onto the brain surface for visualization. It can be roughly seen that for different subjects, their super voxel generation results do not differ much, which indicates that spatial information as well as cluster-level information are more exploited during the super voxel generation process. Moreover, the spatial continuity is calculated for each subject's super voxel generation results, and the spatial dispersion indexes obtained are all 0, i.e., the voxels in each super voxel region are continuous. This phenomenon demonstrates that spatial distance information plays a dominant role in the generation of super voxel voxels, which ensures that the subsequent segmentation of brain regions at the super voxel level is performed on successive regions.

B. Functional segmentation of fMRI at the super voxel level

This paper imports the Graph-Without-Cut (GWC) method raised by Gao et al [13] for functional segmentation of fMRI, which creates an energy minimization function while simultaneously learning the correlation graph and the segmentation results, this method completes the graph construction as well as segmentation in a single step to produce the optimal segmentation results. When compared to graph cut techniques like Ncut [20], it has been demonstrated that GWC performs better. As a result, this paper improves it and extends it from natural images to four-dimensional medical image segmentation tasks for fMRI data.

1) Feature Extraction and Input Map Construction: For the generated super voxels, a feature matrix needs to be developed as the input to the segmentation algorithm. Hence, the feature extraction of fMRI was carried out at the super voxel level in this paper, and a total of four distinct features were tried to be extracted. At first, feature extraction was performed on the spatial location information P of the super voxels. The information P was yielded by calculating the average 3D coordinates of all voxels in this super voxel. Here, the serial number of each voxel along the three axes in fMRI is taken as the coordinate. Then, based on the connection information, the average time series of each hypervoxel is extracted. The histogram of BOLD signal on a total of 215 time slices of each super voxel was calculated for each time series. Furthermore, the Local Binary Pattern(LBP) of the nearest 6 neighbors of all gray matter voxels was also calculated, and the LBP histograms corresponding to all time slices were generated as local features at the super voxel level. For the histograms, 10 columns were used here for calculation.

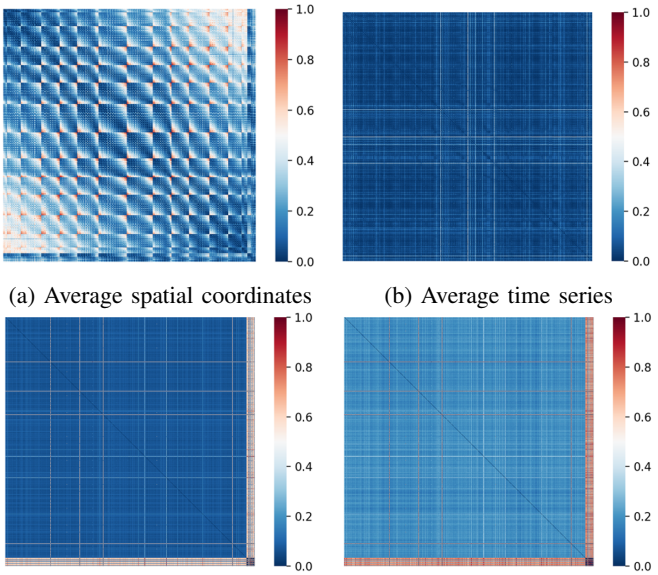

(a) Average spatial coordinates (b) Average time series

(c) BOLD signal histogram (d) LBP histogram

Fig. 4: Feature maps corresponding to the spatial information and feature matrices

The corresponding feature matrices need to be transformed into graphs for the subsequent segmentation algorithm. For each feature matrix, the square of the Euclidean distance between the corresponding feature vectors of the two super voxels was calculated separately, and then transformed into a symmetric square matrix to construct a feature map. Figures 4 describes the feature maps obtained on one subject. It can be seen that all four images are symmetric matrices and the diagonal elements are zero, which is because the correlation between the super voxels is measured here by the Euclidean distance, and the corresponding Euclidean distance between super voxels with a correlation coefficient of 1 is 0. Furthermore, it is noted that among the images constructed

This article has been accepted for publication in IEEE Transactions on Cognitive and Developmental Systems. This is the author's version which has not been fully edited and content may change prior to final publication. Citation information: DOI 10.1109/TCDS.2023.3281271

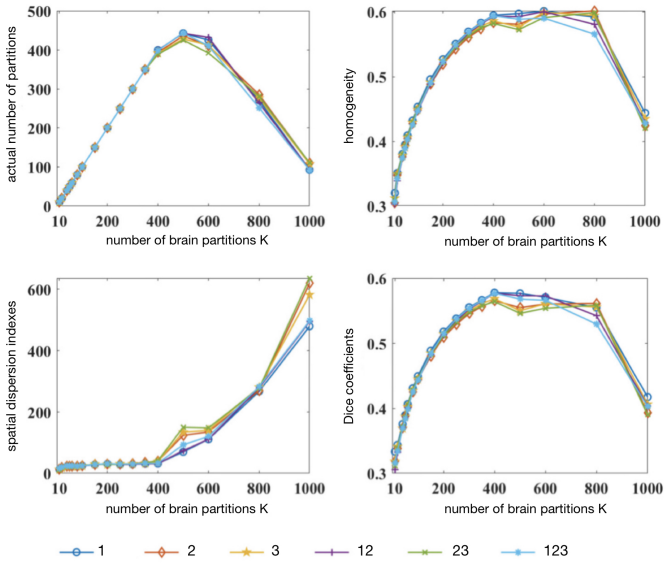

Fig. 5: Comparison of segmentation results under different feature maps

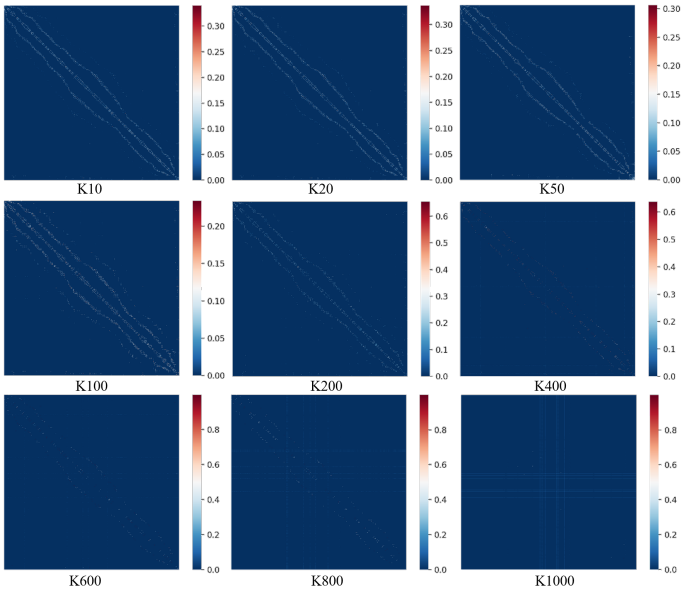

Fig. 6: Visualization of the generated graph G with a preset number of partitions

from the average spatial coordinates, the heat map shows an apparent chunking situation, i.e., the spatial correlation between two neighboring super voxels is small. The reason for this phenomenon is that the super voxels are all generated on the gray matter template as depicted in Figure 1, which contains only part of the voxels of the entire brain, so the two adjacent super voxels are not necessarily contiguous in spatial coordinates. By observing the images constructed from the mean time series, BOLD signal histogram and LBP histogram, it can be found that these three feature maps, especially those corresponding to the BOLD signal histogram and the LBP histogram, have high global similarity, which reflects the correlation between the BOLD signal of voxels and their LBP.

Figure 5 shows the segmentation effects under extracting only the average time series (feature 1), BOLD signal histogram (feature 2), LBP histogram (feature 3), and each feature combination respectively. When the preset number of brain partitions is 400 or less, the segmentation outcomes obtained by distinct feature maps have little difference under several evaluation indexes, which indicates that the segmentation effect is primarily determined by the segmentation algorithm at this time and the impact of features is very small. When the preset number of partitions is above 400, the segmentation results under different feature maps start to differ, and the segmentation effect is slightly better than other feature combinations when combining the average time series with the BOLD signal histogram. Accordingly, for the construction of feature maps in the subsequent experiments, the average spatial coordinates are extracted as the location information, and the average time series as well as the BOLD signal histogram are extracted as the feature information.

In addition, according to the visualization results of gragh G after iterative optimization given in Figure 6, it can be seen that when the number of brain partitions is above 400, the generated connectivity graph is incorrect, indicating that the segmentation results are illogical at this time. Hence, in the subsequent experiments, the number of brain regions would be only set to the value of 400 and below for experimental analysis.

2) Parameter Discussion: In this section, the parameters α and λ in Equation 13 are adjusted to investigate the influence of the weights between the items of the objective function on the segmentation performance of the algorithm. Among them, the meaning of the value of λ is not obvious, but its value can be determined by the number of non-zero elements m in each column of the graph G as mentioned in the previous section. Consequently, in order to make the meaning of the parameter adjustment more clear, the adjustment is performed by adjusting m rather than directly adjusting λ.

The value of α is used to adjust the weights between spatial features and connectivity features in the optimization function. The larger the α value is, the higher the corresponding weights of connectivity features are. When α is small, the segmentation results will over-rely on the spatial information of fMRI and ignore the connectivity information. When α is large, the segmentation results will over-rely on the connectivity information, which may generate many spatially discontinuous partitions. Therefore, the α values were adjusted in the range of 0.05 to 4, and the α values were respectively 0.05,0.1,0.2,0.4,0.8,1,2,4. Among the 40 subjects, the fMRI data of 8 samples were randomly taken for segmentation experiments and the evaluation indexes were calculated to find a α value with better effect.

From Figure 7 we can see that the value of α mainly affects the spatial continuity and reproducibility of the segmentation results. At different preset brain partitions, the effect of varying the value of α on the actual number of brain partitions is almost no influence, and the actual number of brain partitions is equal to the preset number of brain partitions. The value of α also has a small effect on homogeneity. There is no

This article has been accepted for publication in IEEE Transactions on Cognitive and Developmental Systems. This is the author's version which has not been fully edited and content may change prior to final publication. Citation information: DOI 10.1109/TCDS.2023.3281271

regular trend between the spatial continuity of segmentation results and the number of brain subdivisions. Unlike the actual number of brain partitions and the homogeneity index, the value of α exert a greater impact on the spatial continuity of segmentation results. This is due to the fact the larger the value of α, the higher the weight of connection features in the objective function compared to spatial information, so the segmentation algorithm would depend more on similar BOLD timing signals for clustering in the iterative optimization process. For the repeatability of segmentation results, the general trend is that the larger the number of brain partitions, the larger the value of the Dice coefficient. Considering the comprehensive performances of different α values under the above evaluation index, the effect of taking α as 0.1 is better.

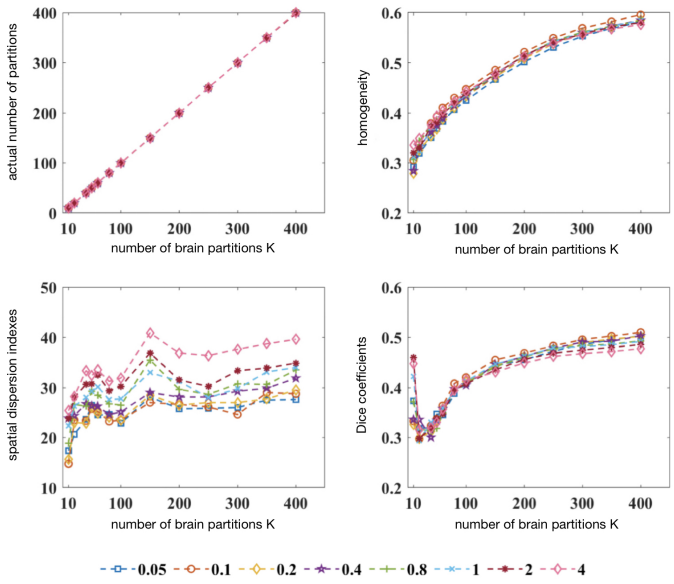

Fig. 7: Effect of α value on segmentation results

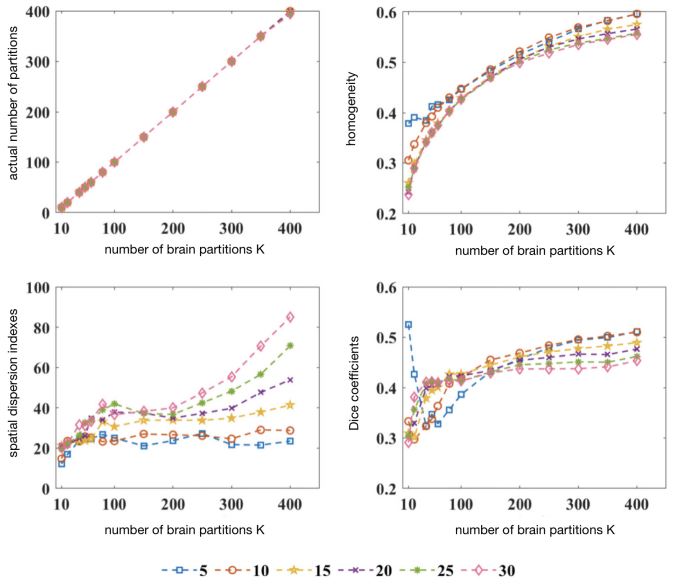

Fig. 8: Effect of m value on segmentation results

The value of m represents the number of nonzero elements of all column vectors in graph G to be optimized. To get a relatively sparse graph G and to segment the super voxels into a predetermined number of partitions, each super voxel must not be connected to too many super voxels. Therefore, m was adjusted in the range of 5 to 30. The values of m were respectively 5,10,15,20,25,30, and the fMRI data of 8 subjects were randomly selected to find a reasonable value of m.

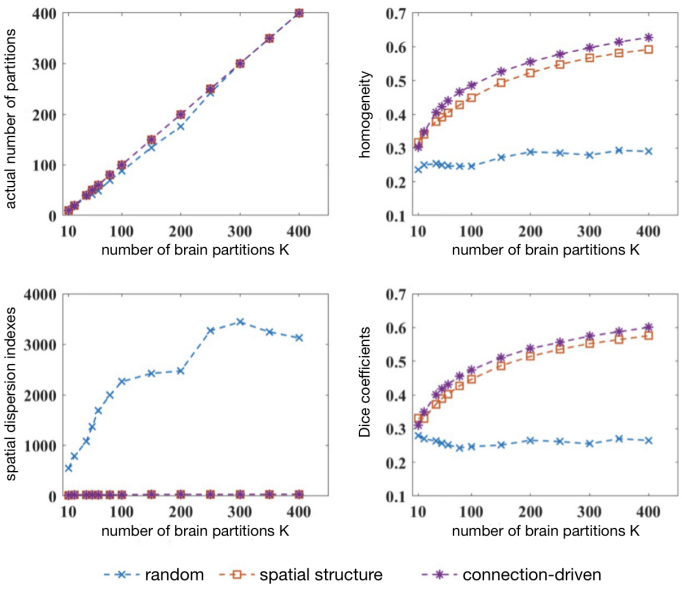

Fig. 9: Experimental comparison of random segmentation and spatial structure-based segmentation

Figure 8 shows that changing the value of m has no influence on the actual number of brain partitions, but has a certain degree of effect on the homogeneity, spatial continuity, and reproducibility of the segmentation results. For the homogeneity index, when the number of brain partitions is 60 or less, the best results are obtained with m value of 5. When the number of brain partitions is between 150 and 300, the best outcomes are achieved with m value of 10. The homogeneity of the segmentation results would be reduced when continuing to increase the value of m. The value of m has a greater impact on the spatial continuity of the segmentation results, and when m is taken as 5 or 10, the index of spatial dispersion basically oscillates back and forth around 25 regardless of the number of brain partitions. However, when m is taken as the rest of the values, the larger the value of m is, the higher the degree of spatial dispersion is in the segmentation with the number of brain partitions more than 200. The value of m also has a certain degree of effect on the reproducibility of the segmentation results. The Dice coefficient displays an overall positive correlation with the number of brain partitions, but some outliers appear when m is taken as 5 or 10 and the number of brain partitions is less than 50, which might be caused by the small number of subject pairs used to assess the reproducibility. Combining the performance of different m values under the above evaluation indexes, the effect is better if m is 10.

This article has been accepted for publication in IEEE Transactions on Cognitive and Developmental Systems. This is the author's version which has not been fully edited and content may change prior to final publication. Citation information: DOI 10.1109/TCDS.2023.3281271

3) Random Segmentation and Spatial Structure-based Segmentation: To further validate that the proposed segmentation algorithm can learn from the connectivity information of fMRI and obtain functional consistent brain partitioning results, random segmentation and segmentation based on spatial structure only were performed on fMRI data under the same experimental settings. Note that the random segmentation means that the average time series at the super voxel level were randomly disorganized and each feature map was calculated based on the randomly disrupted average time series. In addition, the spatial structure-based segmentation refers to using only the spatial location information of the super voxels as the input of the cut-free graph algorithm and ignoring the various connection features of fMRI extracted.

Figure 9 show that the spatial structure-based segmentation and the connection-driven segmentation exhibit similar curves under several evaluation metrics, while the connection-driven segmentation has better segmentation performance in all aspects compared to the random segmentation and the spatial structure-based segmentation. For both connection-driven and spatial structure-based segmentation, the actual number of brain partitions is consistent with the preset number of brain partitions. In contrast, for random segmentation, the actual number of partitions is small when the preset number of partitions is between 50 and 200. In terms of the homogeneity index, the functional coherence of brain regions has the same increasing trend with the increase of the number of brain partitions with both connection-driven segmentation and spatial structure-based segmentation, and the homogeneity value of the former was higher than that of the latter by about 0.35 on average, which indicates that the connection information has a facilitating impact on brain functional segmentation. For the spatial continuity, the brain regions obtained by the connection-driven segmentation and the segmentation based on spatial structure are basically spatially continuous, while the results of the random segmentation have a large degree of spatial dispersion. For the reproducibility of segmentation results, the results of random segmentation are also low, which suggests that similar activation of brain regions exist in different subjects at the same state. Therefore, the functional connectivity information of fMRI is of great importance to ensure the reproducibility of segmentation results.

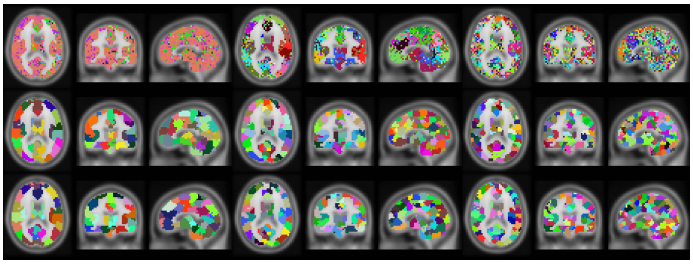

Fig. 10: Comparison of brain maps generated by the three segmentation methods

Figure 10 shows the brain mapping created by a randomly selected subject under three segmentation methods, in which the random, spatial structure-based, and connection-driven

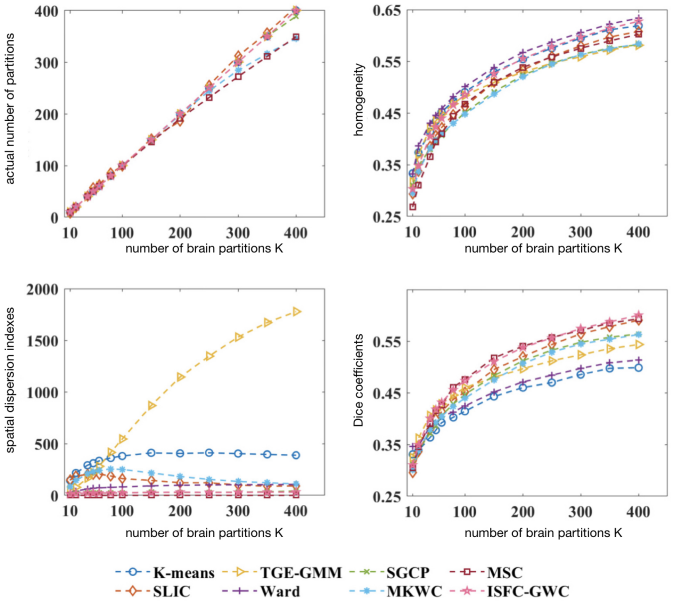

Fig. 11: Comparison of segmentation results of ISFC-GWC and seven clustering algorithms

segmentation results are shown from top to bottom in proper order, and the number of predefined brain regions from left to right are respectively 100, 200 and 400. It is also evident from this brain mapping that both spatial structure-based as well as connection-driven segmentation tend to produce brain regions with relatively uniform size and good continuity, whereas random segmentation yields many brain regions of widely varying and discrete size, which is less efficient in segmentation.

4) Comparison of eight segmentation algorithms: Figure 11 shows the comparison of segmentation results with seven algorithms (K-means, SLIC [21], Ward [22], TGE-GMM [23], SGCP [20], MSC [24], and MKWC [25].). In addition, to more graphically compare the segmentation effects of the different clustering algorithms, Figure 12 shows the kernel density estimates of brain region sizes obtained by the different algorithms, visualized for a preset number of brain partitions of 50, 100, 200, and 400, respectively. In Figures 13 and 14, the brain maps generated by each method are visualized for a randomly selected subject with a preset number of brain partitions of 50, 100, and 200, and the brain maps are visualized in volumetric space and mapped to the surface of the cerebral cortex, respectively.

We can see from Figure 11 that the ISFC-GWC can basically ensure that the actual number of brain partitions is the same as the preset value because the penalty term on the number of brain partitions is added to the optimization function. From the segmentation results of ISFC-GWC in Figure 12, when the preset number of brain regions is 50, 100, 200 and 400, the estimated peak value of brain region size kernel density is about 210, 165, 56 and 38, respectively. The lower the number of voxels in brain regions, the higher the average similarity of their BOLD signals will be, and thus higher functional coherence can be achieved. In addition,

This article has been accepted for publication in IEEE Transactions on Cognitive and Developmental Systems. This is the author's version which has not been fully edited and content may change prior to final publication. Citation information: DOI 10.1109/TCDS.2023.3281271

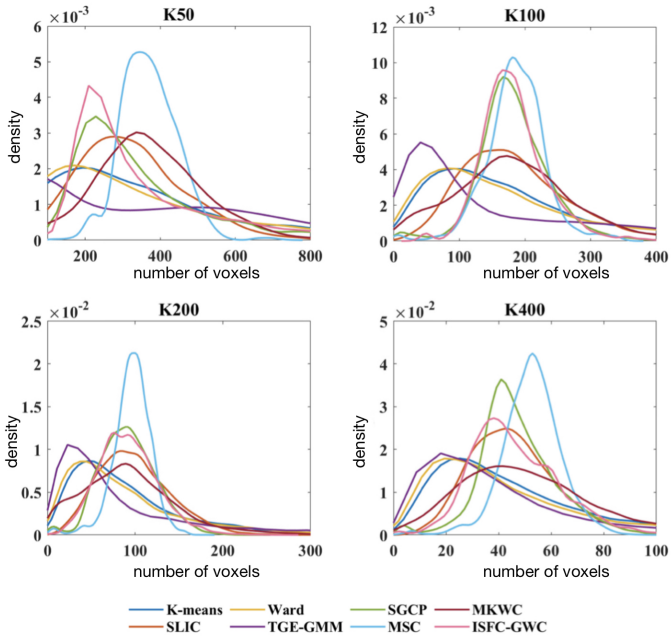

Fig. 12: The kernel density estimates of brain region sizes obtained by different segmentation algorithms

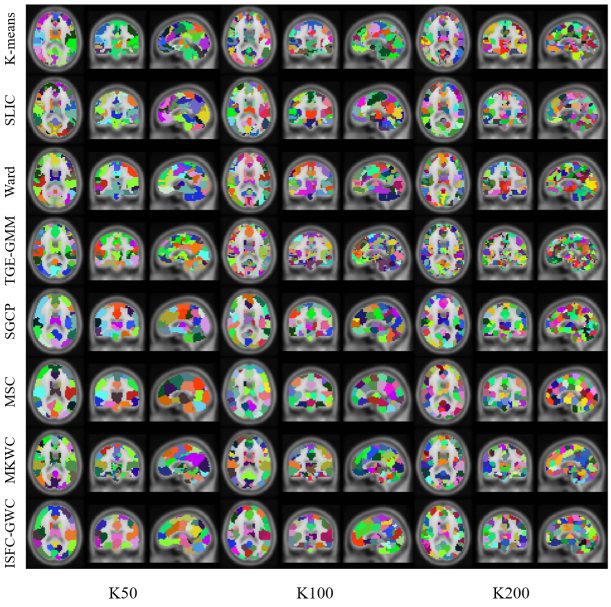

Fig. 13: The brain maps generated by different segmentation algorithms

we can see that the proposed ISFC-GWC algorithm achieved the highest Dice coefficient of 60.05%, indicating that this method can capture more brain state-related cluster features from resting-state fMRI data. Based on the above analysis, the ISFC-GWC is able to generate functional brain regions with the same number of preset brain partitions, and achieves optimal results in terms of reproducibility and suboptimal results in terms of homogeneity and spatial continuity, only slightly lower than the Ward and MSC algorithms respectively. The visualization results of brain volume and brain surface

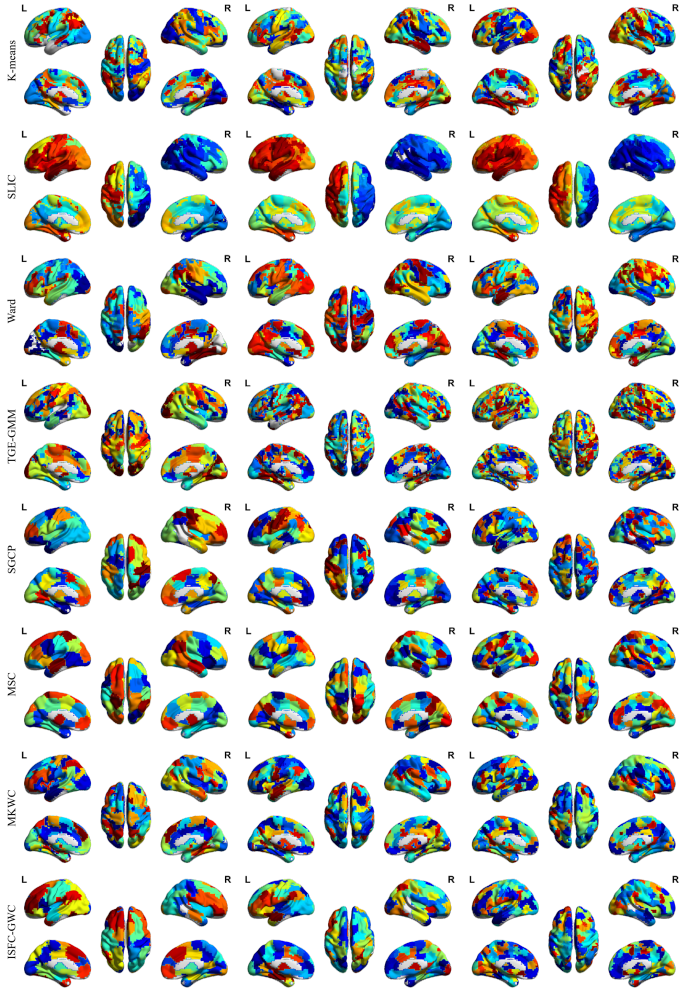

Fig. 14: Brain atlas to cortical surface mapping under eight segmentation algorithms

also describe that the ISFC-GWC generates brain regions that are basically continuous with few discrete points. The shapes of each brain region vary and are not completely constrained by the spatial and structural constraints of the data, but more about the functionality of the voxels.

IV. Conclusion

This paper proposes a connection-driven fMRI segmentation algorithm at the super voxel level, which solves the problem of over-dependence of brain function segmentation on the spatial structure. Moreover, a series of comparison experiments are designed to verify the effectiveness of the ISFC-GWC algorithm. The comparison results with random segmentation and structure-based segmentation illustrate the importance of brain connectivity information for functional segmentation. The comparison results with seven other clustering algorithms on different evaluation metrics demonstrate the advantages of the ISFC-GWC algorithm, which can achieve better spatial continuity and reproducibility and ensure the functional consistency of brain partitioning at the same time. In conclusion, the ISFC-GWC algorithm is an efficient solution

to the problem of whole-brain fMRI functional partitioning at the individual level.

REFERENCES

[1] S. M. Stufflebeam, H. Liu, J. Sepulcre, *et al.*, "Localization of focal epileptic discharges using functional connectivity magnetic resonance imaging," *Journal of neurosurgery*, vol. 114, no. 6, pp. 1693–1697, 2011.

[2] D. Scheinost, J. Benjamin, C. Lacadie, *et al.*, "The intrinsic connectivity distribution: A novel contrast measure reflecting voxel level functional connectivity," *Neuroimage*, vol. 62, no. 3, pp. 1510–1519, 2012.

[3] R. A. N. Nandakumar, D. Hsu and A. Venkataraman, "Deepez: A graph convolutional network for automated epileptogenic zone localization from resting-state fmri connectivity," *IEEE Transactions on Biomedical Engineering*, vol. 70, no. 1, pp. 216–227, 2023.

[4] D. S. Bassett, E. Bullmore, B. A. Verchinski, *et al.*, "Hierarchical organization of human cortical networks in health and schizophrenia," *Journal of Neuroscience*, vol. 28, no. 37, pp. 9239–9248, 2008.

[5] K. Supekar, V. Menon, D. Rubin, *et al.*, "Network analysis of intrinsic functional brain connectivity in alzheimer's disease," *PLoS Computational Biology*, vol. 4, no. 6, p. e1000100, 2008.

[6] Y. Zhao *et al.*, "Four-dimensional modeling of fmri data via spatio-temporal convolutional neural networks (st-cnns)," *IEEE Transactions on Cognitive and Developmental Systems*, vol. 12, no. 3, pp. 451–460, 2020.

[7] B. Sen and K. K. Parhi, "Predicting biological gender and intelligence from fmri via dynamic functional connectivity," *IEEE Transactions on Biomedical Engineering*, vol. 68, no. 3, pp. 815–825, 2021.

[8] Z. Wang *et al.*, "Distribution-guided network thresholding for functional connectivity analysis in fmri-based brain disorder identification," *IEEE Journal of Biomedical and Health Informatics*, vol. 26, no. 4, pp. 1602–1613, 2022.

[9] W. Zhang *et al.*, "Experimental comparisons of sparse dictionary learning and independent component analysis for brain network inference from fmri data," *IEEE Transactions on Biomedical Engineering*, vol. 66, no. 1, pp. 289–299, 2019.

[10] M. Pakravan and M. B. Shamsollahi, "Joint, partially-joint, and individual independent component analysis in multi-subject fmri data," *IEEE Transactions on Biomedical Engineering*, vol. 67, no. 7, pp. 1969–1981, 2020.

[11] F. L *et al.*, "The human brainnetome atlas: A new brain atlas based on connectional architecture," *Cereb Cortex*, vol. 26, no. 8, pp. 3508–3526, 2016.

[12] M. Schmidt and K. Alahari, "Generalized fast approximate energy minimization via graph cuts: Alpha-expansion beta-shrink moves," in *27th Conference on Uncertainty in Artificial Intelligence*, 2011.

[13] L. Gao, J. Song, F. Nie, *et al.*, "Graph-without-cut: An ideal graph learning for image segmentation," in *Proceedings of the AAAI Conference on Artificial Intelligence*, 2016.

[14] F. Nie, X. Wang, and H. Huang, "Clustering and projected clustering with adaptive neighbors," in *Proceedings of the 20th ACM SIGKDD international conference on Knowledge discovery and data mining*, pp. 977–986, 2014.

[15] B. Mohar, "The laplacian spectrum of graphs," *Graph Theory, Combinatorics, and Applications*, vol. 2, pp. 871–898, 1991.

[16] R. Achanta, A. Shaji, K. Smith, *et al.*, "Slic superpixels compared to state-of-the-art superpixel methods," *IEEE Transactions on Pattern Analysis and Machine Intelligence*, vol. 34, no. 11, pp. 2274–2282, 2012.

[17] J. Wang and H. Wang, "A supervoxel-based method for groupwise whole brain parcellation with resting-state fmri data," *Frontiers in human neuroscience*, 2016.

[18] W. Wu, A. Y. Chen, L. Zhao, *et al.*, "Brain tumor detection and segmentation in a crf (conditional random fields) framework with pixel-pairwise affinity and superpixel-level features," *International journal of computer assisted radiology and surgery*, vol. 9, no. 2, pp. 241–253, 2014.

[19] Y. Kong, J. Wu, G. Yang, *et al.*, "Iterative spatial fuzzy clustering for 3d brain magnetic resonance image supervoxel segmentation," *Journal of neuroscience methods*, vol. 311, pp. 17–27, 2019.

[20] J. Wang, Z. Hao, and H. Wang, "Generation of individual whole-brain atlases with resting-state fmri data using simultaneous graph computation and parcellation," *Frontiers in human neuroscience*, vol. 12, p. 166, 2018.

[21] J. Wang, Z. Hu, and H. Wang, "Parcellating whole brain for individuals by simple linear iterative clustering," in *International Conference on Neural Information Processing*, pp. 131–139, 2016.

[22] B. Thirion, G. Varoquaux, E. Dohmatob, *et al.*, "Which fmri clustering gives good brain parcellations?," *Frontiers in Neuroscience*, vol. 8, no. 167, 2014.

[23] M. Azimbagirad and L. O. M. Junior, "Tsallis generalized entropy for gaussian mixture model parameter estimation on brain segmentation application," *Neuroscience Informatics*, vol. 1, no. 1-2, p. 100002, 2021.

[24] R. C. Craddock, G. A. James, P. E. Holtzheimer Iii, *et al.*, "A whole brain fmri atlas generated via spatially constrained spectral clustering," *Human brain mapping*, vol. 33, no. 8, pp. 1914–1928, 2012.

[25] X. Shen, F. Tokoglu, X. Papademetris, *et al.*, "Groupwise whole-brain parcellation from resting-state fmri data for network node identification," *Neuroimage*, vol. 82, pp. 403–415, 2013.

Kevin W. Tong is currently working towards the Ph.D. Degree in School of Mechanical Engineering, Nanjing University of Science and Technology. His research interests include deep learning, human-machine interaction, medical image analysis, brain cognition and 3D reconstruction.

Xiao-Yan Zhao received the master's degree in medicine from Southeast University, Nanjing, China,in 2012.

She is currently as a Attending Doctor of rehabilitation medicine with Anhui No.2 Provincial People's Hospital, Hefei, China. Her research interests include rehabilitation of neurological diseases, especially in Alzheimer disease, and cerebrovascular disease.

Yong-Xia Li received her M.Sc in Emergency medicine from Shanghai Jiao Tong University School of Medicine. She is now a attending physician in Department of Emergency, Shanghai sixth people's hospital. Her research interests include Septic encephalopathy, postoperative delirium, Differential diagnosis of coma, Intensive care unit syndrome.

Ping Li (Member, IEEE) received the Ph.D. degrees in biomedical engineering from Southeast University, Nanjing, China, in 2003. She is a professor in School of biological science and medical engineering at Beihang University. Her research interests include magnetically actuated hydrogel robots, magnetoelectric bifunctional tissue engineering scaffolds, repair of nerve, bone and skin tissue under mechanical-electrical or magnetoelectric stimulation.